RSC Advances

PAPER

View Article Online
View Journal | View Issue

Cite this: *RSC Adv.*, 2022, **12**, 6186

Facile synthesis of nanostructured perovskites by precursor accumulation on nanocarbons†

Mai Higuchi,‡ Mizuri Yaguchi,‡ Miru Yoshida-Hirahara, Hitoshi Ogihara * and Hideki Kurokawa

Received 15th November 2021
Accepted 14th February 2022

DOI: 10.1039/d1ra08357k

rsc.li/rsc-advances

Perovskite-type oxides have impacted various research fields, including materials and energy science. Despite their vast potential in various applications, general and simple synthesis methods for nano-perovskites remain limited. Herein, various nano-perovskites were synthesized by a facile approach involving the use of nanocarbons. The calcination of the nanocarbon deposited with metal salts yielded nano-perovskites, emulating the morphology of nanocarbons. The accumulation of precursors (*i.e.*, metal salts) on the surface of the nanocarbon during the evaporation of the solvent is the key step in which the precursors are homogeneously mixed prior to calcination. The homogeneity of the precursors facilitated low-temperature calcination that resulted in the formation of nano-perovskites. Various nano-perovskites, including $LaMnO_3$, $LaCoO_3$, $LaFeO_3$, $LaNiO_3$, $LaAlO_3$, $LaGaO_3$, $CaMnO_3$, $BaMnO_3$, $SrMnO_3$, $La_{0.7}Sr_{0.3}FeO_3$, La_2CuO_4, and $Ca_2Fe_2O_5$, were successfully synthesized, demonstrating the simplicity and novelty of the method for the general synthesis of nano-perovskites.

1. Introduction

Perovskite-type oxides are a class of materials that exhibit unique and superior properties, including dielectric, magnetic, ionic, and electronic transport; therefore, they show tremendous potential in various applications such as solar cells, catalysts, sensors, and fuel cells.[1–9] Chemically, perovskites are oxides with an ABO_3 type structure in which a wide variety of A- and B-site cations can be incorporated; thus, they are considered functionally versatile. To synthesize perovskites, the A- and B-site cations must be uniformly distributed in the oxide structure. Classical solid-state synthesis is a widely used method in which the precursor (typically a single metal oxide) is physically ground and calcined at high temperatures. Despite its simplicity, the solid-phase method has disadvantages, such as sintering of perovskite during high-temperature calcination and decreased surface area of perovskite due to the formation of large particles, which are undesirable for some applications such as catalysts. In the solid-phase method, the diffusion of cations into the crystalline state at high temperatures is the driving force for the formation of perovskites. However, high-temperature calcination must be avoided during the synthesis of nano-perovskites. Here, a precursor in which different cations are uniformly distributed is beneficial. The pre-mixing of A- and B-site cations allows the formation of a mixed-oxide structure by low-temperature calcination, as long-distance diffusion of cations into solids is no longer required.

The sol–gel method is a wet process that has been developed based on the aforementioned strategy.[10–13] Typically, a chelating reagent (*e.g.*, citrate) and a polyol are used to crosslink A- and B-site cations and form a gel with uniformly distributed metal cations. The low-temperature calcination of the gel yielded nanosized perovskites. In addition to the sol–gel method, other solution-based approaches, such as coprecipitation,[10,14,15] combustion,[16–18] flame-spray,[19–22] and microemulsion methods,[23,24] have been explored. Recently, other novel processes to synthesize nano-perovskites have also been reported, such as solid-state gelation and molten-salt-protected pyrolysis.[25–28]

Our research group has developed a new strategy, the precursor accumulation (PA) method, to synthesize nanostructured oxides (Scheme 1).[29–34] Typically, a metal precursor solution is dropped onto the nanocarbon powder, followed by solvent evaporation, which leaves the precursor on the surface of the nanocarbon. Subsequently, the calcination process removes the nanocarbon, yielding nanostructured oxides that emulate the nanocarbon morphology. Using nanocarbons as the carbon source, the PA method has enabled the synthesis of monoxide nanotubes (SiO_2, Al_2O_3, ZrO_2, NiO, Fe_2O_3)[29,30] and perovskites ($LaMnO_3$).[31] Recently, we reported the synthesis of $LaCoO_3$ by the PA method and clarified that the impurities contained in the carbon sources negatively affect the formation of $LaCoO_3$.[34] However, it was still unclear if the PA method can be applied to synthesize versatile perovskites. As mentioned

Graduate School of Science and Engineering, Saitama University, 255 Shimo-Okubo, Sakura-ku, Saitama 338-8570, Japan. E-mail: ogihara@mail.saitama-u.ac.jp

† Electronic supplementary information (ESI) available. See DOI: 10.1039/d1ra08357k

‡ These authors contributed equally to this work.

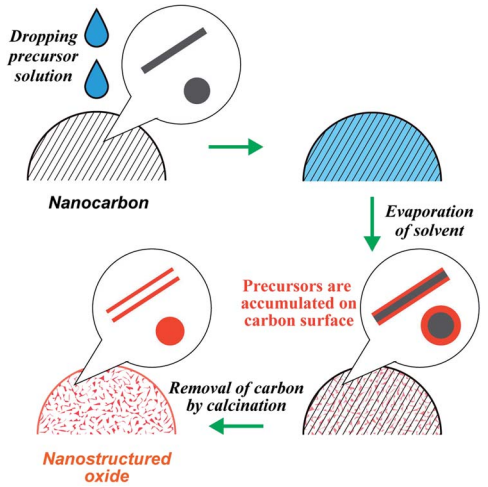

Scheme 1 Schematic diagram of the precursor accumulation (PA) method.

earlier, there are various methods for the synthesis of nano-perovskites; however, general and straightforward routes are still limited. Herein, we demonstrate that the PA method could be an effective approach for the facile synthesis of a wide variety of nano-perovskites.

2. Experimental section

2.1 Materials

$La(NO_3)_3 \cdot 6H_2O$, $Ca(NO_3)_2 \cdot 4H_2O$, $Ba(CH_3COO)_2$, $Mn(NO_3)_2 \cdot 6H_2O$, $Ga(NO_3)_3 \cdot nH_2O$, $Co(NO_3)_2 \cdot 6H_2O$ (Wako Pure Chemical Industries, Ltd), $Ca(CH_3COO)_2 \cdot H_2O$, $Sr(NO_3)_2$, $Sr(CH_3COO)_2 \cdot 0.5H_2O$, $Mn(CH_3COO)_2 \cdot 4H_2O$, $Fe(NO_3)_3 \cdot 9H_2O$, $Ni(NO_3)_2 \cdot 6H_2O$, $Al(NO_3)_3 \cdot 9H_2O$, and ethanol (Kanto Chemical Co., Inc.) were used as received. Ketjen black (KB; Lion Specialty Chemicals Co., Ltd) and carbon nanofibers (CNFs; graphitized, iron-free; Sigma-Aldrich) were used as carbon sources for the PA method. The carbons were used as received when ethanol was used as the solvent. When water was used as the solvent, KB was calcined in air for 4 h at 773 K. The calcination process was aimed at enhancing the wettability of carbon to water by introducing oxygen-containing functional groups.

2.2 Synthesis of perovskites *via* the PA method

A schematic of the PA method is shown in Scheme 1. As an example, the synthesis procedure of $LaMnO_3$ is shown below. $La(NO_3)_3 \cdot 6H_2O$ (0.6495 g) and $Mn(NO_3)_2 \cdot 6H_2O$ (0.4306 g) were dissolved in ethanol to be 10 mL of the precursor solution. We previously reported the synthesis of $LaCoO_3$ by the PA method and found that KB and CNFs were suitable carbon sources to obtain a pure perovskite structure because KB and CNFs contain no impurities.[34] Thus, we used KB and CNFs in this study. 0.2 g of carbon (KB or CNFs) was placed on a funnel (Kiriyama Glass Works Co.; 21 mm diameter) with a membrane filter (ADVANTEC, PTFE, pore size: 0.2 μm). A sufficient amount of the precursor solution (approximately 5 mL) was dropped onto the carbon powder. The volume of the dropped precursor solution was much larger than the volume of the carbon source. Excess solvent was removed *via* suction filtration. The solvent that penetrated the carbon powder was dried by suction filtration for 1 h. The resulting sample was placed in a convection oven at 403 K overnight and ground using a mortar. The obtained composite of the precursors and carbon was placed in a crucible and heated in an electric furnace in air. The temperature of the furnace was elevated over 2 h and maintained for 4 h. After calcination at 873 K, the carbons were removed ($C + O_2 \rightarrow CO_2$), and $LaMnO_3$ were formed. For the synthesis of other perovskites, all samples were prepared in a similar way and the details (*e.g.*, types of precursor, solvent, drying temperature, and calcination temperature) are shown in Table S1.†

2.3 Sample preparation without using nanocarbons

A solution containing metal salts was prepared. The solution was first heated in a crucible on a hot plate at 363–383 K, and the solvent (ethanol or water) was evaporated. The resulting sample was then calcined in air. Details of the preparation conditions are listed in Table S1.†

2.4 Characterization

X-ray diffraction (XRD) patterns of the synthesized samples were recorded with a D2 Phaser (Bruker) using Cu Kα radiation. The crystalline sizes of the perovskites were determined using the Scherrer equation.

Thermal gravimetry/differential thermal analysis (TG/DTA) was performed using a DTG-60 (Shimadzu Corp.). Under flowing air, the sample was heated to 1073 K at 10 K min^{-1}.

Nitrogen adsorption/desorption measurements were performed on a Belsorp II (MicrotracBEL) sorption analyzer at 77 K. Before the measurements, samples were degassed under vacuum at 573 K for 30 min. The specific surface area was calculated using the Brunauer–Emmett–Teller equation.

Field emission scanning electron microscopy (FE-SEM) images were obtained using an S-4800 (Hitachi High-Technologies Corporation) operated at 15 kV. Before the SEM measurements, the samples were coated with a few nanometers of Pt–Pd to reduce charge accumulation.

Transmission electron microscopy (TEM) was performed on a Tecnai G2 20 (FEI Co.) instrument operated at an acceleration voltage of 200 kV. The sample was ultrasonically dispersed in ethanol, and a few drops of the suspension were deposited onto carbon-coated copper TEM grids. After drying the grids in air, the TEM measurements were performed.

Scanning transmission electron microscopy (STEM) and energy-dispersive X-ray spectroscopy (EDX) were performed on a JEM-ARM200F-B (JEOL Ltd, Japan) instrument operated at an acceleration voltage of 200 kV. The sample for STEM/EDX analysis was prepared using the following procedure: $La(NO_3)_3 \cdot 6H_2O$ and $Mn(NO_3)_2 \cdot 6H_2O$ were accumulated on the CNFs using the procedure described in Section 2.2. The sample was calcined in air at 573 K, in which the CNFs were not combusted, and the metal nitrates were partly decomposed. The

purpose of calcination is to avoid the dissolution of metal nitrates during sonication in ethanol. The accumulation/calcination process was repeated five times to intensify the EDX signal. The sample was then ultrasonically dispersed in ethanol, and a few drops of the suspension were deposited onto carbon-coated copper TEM grids. After drying the grids in air, STEM/EDX measurements were performed.

3. Results and discussion

Commercially available carbon black (KB) and carbon nanofibers (CNFs) were used as carbon sources. After dropping the precursor solution of metal salts (metal nitrates or acetates) onto the nanocarbon, the sample was dried and calcined in air (Scheme 1). During the calcination process (873–1073 K), the nanocarbon was combusted, and a perovskite was formed. The minimum calcination temperature was 873 K. This temperature was increased when the perovskite structure was not detected in the XRD analysis.

Fig. 1 shows the XRD patterns of the prepared samples ($LaMnO_3$, $LaCoO_3$, $LaFeO_3$, $LaNiO_3$, $LaAlO_3$, $LaGaO_3$, $CaMnO_3$, $BaMnO_3$, $SrMnO_3$, and $La_{0.7}Sr_{0.3}FeO_3$). Distinct peaks of the perovskite structure (ABO_3) are observed. In addition, brownmillerite ($Ca_2Fe_2O_5$) and Ruddlesden–Popper (La_2CuO_4) phases were observed. Although tiny peaks for other oxides such as $La_4Ga_2O_9$ and $Ca_2Mn_3O_8$ were observed, they were minor phases. Table 1 lists the physicochemical properties of the synthesized perovskites. The crystallite sizes estimated from the XRD patterns were in the range of 13–48 nm, indicating that the perovskites consisted of nanocrystallites. The specific surface area ranged from 4 to 44 $m^2\ g^{-1}$, which is comparable to that of nano-perovskites synthesized by conventional liquid-phase methods (Table S2†). Furthermore, the adsorption/desorption isotherm for $LaMnO_3$ showed a typical type II isotherm (Fig. S1†), indicating that $LaMnO_3$ has no micro- or mesopores. These results strongly suggest that the PA method yields a wide variety of perovskites with high surface areas. The loading of perovskites to the carbon source can be estimated by the weight of the used carbon and the formed perovskites. For example, 54 mg of $LaNiO_3$ were obtained when 201 mg of KB were used, indicating that the loading of $LaNiO_3$ to KB was 21 wt%. For the other samples, the loadings of the perovskites were approximately 20 wt%.

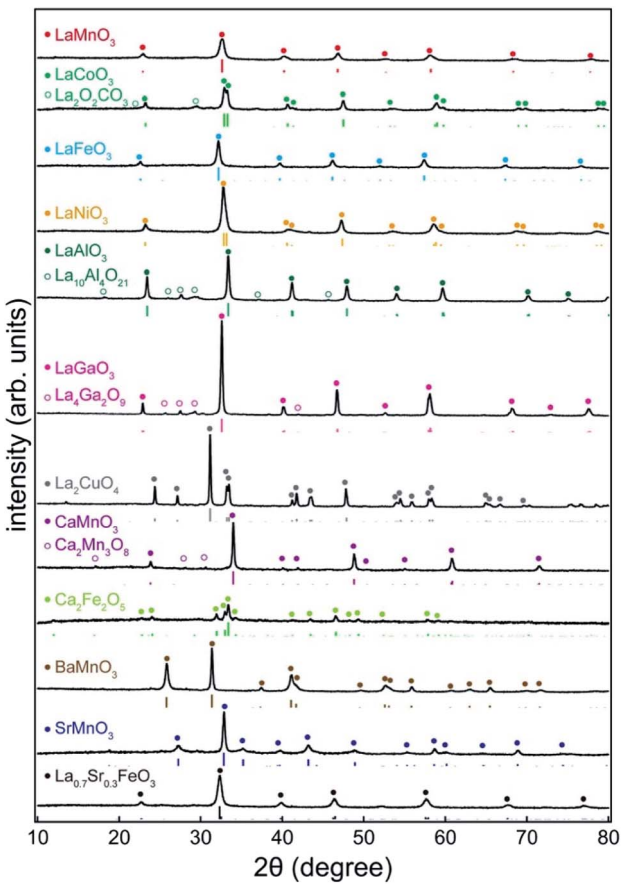

Fig. 1 XRD patterns of perovskites prepared by the PA method using KB as the carbon source. The XRD patterns were indexed as $LaMnO_3$, $LaCoO_3$, $LaFeO_3$, $LaNiO_3$, $LaAlO_3$, $LaGaO_3$, La_2CuO_4, $CaMnO_3$, $Ca_2Fe_2O_5$, $BaMnO_3$, $SrMnO_3$, and $La_{0.7}Sr_{0.3}FeO_3$ using JCPDS card no. 75-0440, 84-0848, 37-1493, 70-5757, 31-0022, 24-1102, 82-2142, 89-0666, 47-1744, 26-0168, 24-1213, and 89-1269, respectively.

Fig. 2 shows SEM images of KB and the synthesized perovskites. KB is composed of nanoparticles of approximately 20–50 nm (Fig. 2a). The synthesized $SrMnO_3$ and $LaMnO_3$ using KB were nanoparticles (Fig. 2b and c), and the other perovskites also exhibited nanoparticle structures (Fig. S2†). In contrast, the perovskites prepared using CNFs exhibited a fibrous morphology. For example, $LaFeO_3$ was observed (Fig. 2d) with a fibrous morphology ($d \sim 100$ nm) similar to that of the CNFs (Fig. S3a†). The TEM image (inset: Fig. 2d) clearly shows that $LaFeO_3$ is a nanotube, indicating that the CNFs acted as a template. The other perovskites also possessed fibrous structures (Fig. S3b–f†). It should be noted that perovskite structures and high surface areas were observed in all samples prepared using CNFs (Fig. S4 and Table S3†), and the perovskite nanoparticles prepared using KB were not hollow structures (Fig. S5†). From Fig. S5,† we can see that the lattice fringe of $LaMnO_3$ and the size of $LaMnO_3$ crystallite was approximately

Table 1 Crystallite size and specific surface area of the perovskites prepared by the PA method using KB as the carbon source. Crystallite sizes were evaluated from XRD patterns using Scherrer's equation

Perovskite	Crystallite size (nm)	Specific surface area ($m^2\ g^{-1}$)
$LaMnO_3$	13	44
$LaCoO_3$	24	24
$LaFeO_3$	20	36
$LaNiO_3$	16	7
$LaAlO_3$	29	24
$LaGaO_3$	35	4
La_2CuO_4	48	4
$CaMnO_3$	37	5
$Ca_2Fe_2O_5$	35	32
$BaMnO_3$	37	9
$SrMnO_3$	28	10
$La_{0.7}Sr_{0.3}FeO_3$	15	33

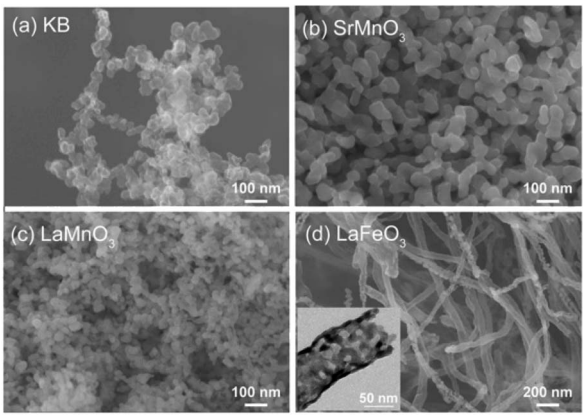

Fig. 2 SEM images of (a) KB, (b) $SrMnO_3$, (c) $LaMnO_3$, and (d) $LaFeO_3$. Inset of (d): TEM image of $LaFeO_3$. Carbon sources: KB (b and c), and CNFs (d).

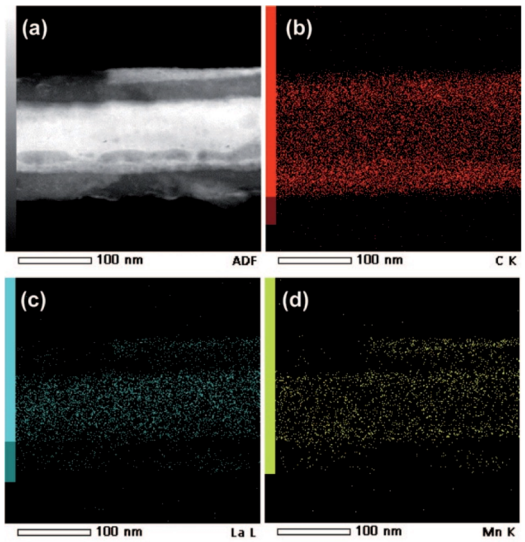

Fig. 3 STEM (a) and EDX elemental mapping images for (b) C, (c) La, and (d) Mn. The processes of nitrate deposition and calcination at 573 K were repeated 5 times prior to STEM/EDX analyses.

10 nm, which was almost the same as the crystallite size calculated from the XRD pattern (13 nm shown in Table 1). The notable effect of the carbon source on the morphology of perovskites suggests that perovskite synthesis proceeds with the aid of nanocarbons. As discussed later, the precursors accumulate on the surface of the nanocarbon, so that the corresponding perovskites inherit the morphological characteristics of the nanocarbon after its removal.

In order to explain the role of nanocarbons, perovskite synthesis was attempted without using a carbon source. Although some samples exhibited perovskite structures, impurity phases ($La(OH)_3$, La_2O_3, $BaCO_3$, and $SrCO_3$) dominantly formed in the rest (Fig. S6†). Furthermore, the specific surface areas of these samples were lower than those of the perovskites prepared using nanocarbons (Table S4†) because of the larger particles (Fig. S7†). Thus, by comparing the physicochemical properties of the samples prepared with and without nanocarbons, it can be concluded that nanocarbons are indispensable for the synthesis of nano-perovskites.

Microscopic analyses were performed to study the distribution state of the precursors on the nanocarbons. Lanthanum and manganese nitrates were deposited on the surface of the CNFs and calcined at 573 K without combustion of the CNFs. Fig. 3 shows the STEM and EDX images of the samples. In the EDX elemental mappings (Fig. 3b–d), the signals for La and Mn evenly overlapped with those for C, indicating that the different metal precursors did not segregate on the carbon. These results strongly suggest that the different precursors were homogeneously deposited on the CNFs *via* the PA method.

Furthermore, the pre-mixing of precursors on nanocarbons prevented the formation of impurity phases. Fig. 4 shows the XRD patterns of the samples synthesized from a mixture of lanthanum and manganese nitrates (a–d), lanthanum nitrate (e), and manganese nitrate (f) deposited on KB. It was observed that the calcination at 793 K did not provide a perovskite structure, and the peaks of $LaMnO_3$ only appeared at 823–873 K. Regardless of the calcination temperature, no impurity phases such as single oxides were observed. It should be emphasized that samples (e) and (f) calcined at 793 K exhibited distinct diffraction peaks of Mn_2O_3, Mn_3O_4, and $(LaO)_2CO_3$. The XRD patterns demonstrated that under the same conditions in which a single precursor turned into a single oxide or carbonate (samples (e) and (f)), the simultaneous deposition of both precursors yielded only a perovskite structure (sample (a–c)). As shown earlier in the STEM/EDX images, the two precursors remained homogeneously mixed on the surface of nanocarbon, that is, the precursors did not segregate. It is clear that under such conditions, the formation of perovskite from different

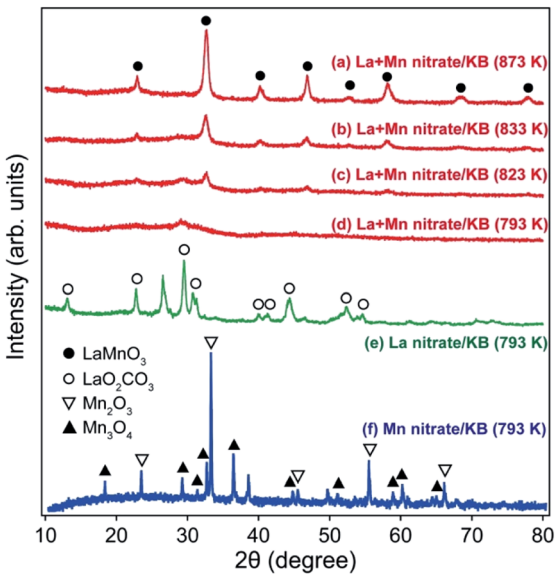

Fig. 4 XRD patterns of the samples prepared by the deposition of (a–d) a mixture of lanthanum and manganese nitrates, (e) lanthanum nitrate, and (f) manganese nitrate on KB, following calcination at different temperatures.

cations is more likely to occur than the aggregation of identical ions to form single metal products.

Based on the characterization results, we propose a synthesis mechanism for the PA method (Scheme 2). In this method, a solution of different precursors was dropped onto the nanocarbon substrate, and the solvent was evaporated. During the evaporation process, the precursors were left on the surface of the nanocarbon. STEM/EDX analyses suggested that the precursors were homogeneously mixed on the surface of the nanocarbons. XRD analyses indicated that the mixed state of the precursors prevented the aggregation of single precursor ions, which could otherwise form impurity phases such as single metal oxides. The homogeneity of the precursors results in the formation of mixed oxides (*i.e.*, perovskites) because, similar to the sol–gel method, the mixed state of precursors helps to form perovskites during low-temperature calcination. In addition, without the carbon substrate, impurity phases were formed (Fig. S6†), indicating the significant role of nanocarbon in homogenizing the precursors.

The other significant effect of nanocarbon is the control of the morphology of perovskites. The perovskites exhibited a morphology similar to that of the carbon sources (Fig. 2, S2, and S3†) because the precursors on the nanocarbons were converted into perovskites (Scheme 2). By emulating the morphology of the carbon source, the formed perovskites showed nanostructures such as nanoparticles or nanotubes with a high surface area.

Fig. S8† shows TG/DTA for KB and precursor/KB samples. The accumulation of metal salts affects the combustion behavior of the KB. An exothermic peak was observed for the combustion of KB at 935 K, which shifted to a lower temperature (620–710 K) in the presence of the precursors. This shift indicates that the metal salt precursors promoted the combustion of KB. Considering the fact that the formation of $LaMnO_3$ occurred at temperatures $\geq$ 823 K (XRD patterns; Fig. 4) and the combustion of KB was complete well within 773 K for the (La + Mn)/KB sample (TG/DTA profile), it can be stated that KB entirely disappeared before the formation of the perovskite structure. This fact supports the following assumptions: (1) the heat of combustion of the carbon source does not affect the formation of the perovskite structure, and (2) the carbon source does not remain in perovskites; thus, the high surface area of the perovskites cannot be ascribed to the carbon sources. Indeed, the TG profile of $LaMnO_3$ exhibited no weight loss (Fig. S9†), indicating that $LaMnO_3$ does not contain a carbon source.

Finally, it is essential to highlight the differences between PA and conventional wet methods. The fundamental difference is that the PA method does not rely on chemical reactions to homogenize the precursors. For example, in the sol–gel method, chelating reagents and polyols are used for complex formation and polycondensation reactions, which results in a gel with homogeneously mixed precursors.[11] The coprecipitation method requires chemical agents such as sodium hydroxide,[14] while organic compounds such as glycine are necessary for combustion methods.[18] In contrast, the PA method requires only the metal salts and nanocarbons. Therefore, the novelty of this method is the use of nanocarbons instead of chemical reagents to facilitate the mixing of the precursors.

Furthermore, the deposition of precursors on nanocarbons imparts the PA method the simplicity of producing a variety of perovskites. Because the physical deposition process is hardly affected by the type of precursor, it can be assumed that various precursors can be homogeneously deposited on the nanocarbon without the need for precise control over the preparation conditions.

The salient features of the PA method are as follows: (1) no specific reagent is required except for the metal salts and commercially available nanocarbon, (2) no special equipment is required, and (3) no harsh conditions are involved as the process occurs at moderate temperature and atmospheric pressure.

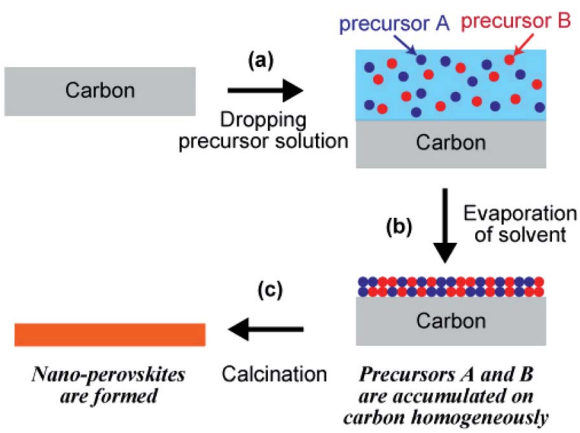

Scheme 2 Schematic diagram of precursor accumulation process on the carbon substrate.

4. Conclusions

In summary, the precursor accumulation (PA) method, a general and straightforward synthesis route for nano-perovskites, was developed. Nano-perovskites were prepared by dropping a precursor solution of metal salts into the nanocarbon powder, followed by drying and calcination in air. This method provides a variety of perovskites. The formed perovskites exhibited nanostructures such as nanoparticles and nanofibers, emulating the morphology of the corresponding carbon source. The PA method is different from other conventional methods (*e.g.*, solid-state method and sol–gel method) in terms of ease of synthesis, and is expected to be a method of choice for the facile synthesis of nano-perovskites.

Conflicts of interest

There are no conflicts to declare.

Acknowledgements

We acknowledge the Comprehensive Analysis Center for Science at Saitama University for technical support with the XRD, SEM, and TEM analyses. This work was partially supported by JSPS KAKENHI (Grant numbers JP18K04832, JP21H01710, and JP21K05193) and the TEPCO Memorial Foundation. A part of this work was supported by the NIMS microstructural characterization platform as a program of the "Nanotechnology Platform" of the Ministry of Education, Culture, Sports, Science and Technology (MEXT), Japan.

Notes and references

1 D. J. Chen, C. Chen, Z. M. Baiyee, Z. P. Shao and F. Ciucci, *Chem. Rev.*, 2015, **115**, 9869–9921.
2 M. A. Green, A. Ho-Baillie and H. J. Snaith, *Nat. Photonics*, 2014, **8**, 506–514.
3 K. Kamata, *Bull. Chem. Soc. Jpn.*, 2019, **92**, 133–151.
4 A. Kojima, K. Teshima, Y. Shirai and T. Miyasaka, *J. Am. Chem. Soc.*, 2009, **131**, 6050–6051.
5 M. A. Pena and J. L. G. Fierro, *Chem. Rev.*, 2001, **101**, 1981–2017.
6 J. Suntivich, K. J. May, H. A. Gasteiger, J. B. Goodenough and Y. Shao-Horn, *Science*, 2011, **334**, 1383–1385.
7 J. W. Zhao, Z. X. Shi, C. F. Li, Q. Ren and G. R. Li, *ACS Mater. Lett.*, 2021, **3**, 721–737.
8 N. Kumar, M. Kumar, T. C. Nagaiah, V. Siruguri, S. Rayaprol, A. K. Yadav, S. N. Jha, D. Bhattacharyya and A. K. Paul, *ACS Appl. Mater. Interfaces*, 2020, **12**, 9190–9200.
9 N. Kumar, K. Naveen, M. Kumar, T. C. Nagaiah, R. Sakla, A. Ghosh, V. Siruguri, S. Sadhukhan, S. Kanungo and A. K. Paul, *ACS Appl. Energy Mater.*, 2021, **4**, 1323–1334.
10 B. L. Cushing, V. L. Kolesnichenko and C. J. O'Connor, *Chem. Rev.*, 2004, **104**, 3893–3946.
11 A. E. Danks, S. R. Hall and Z. Schnepp, *Mater. Horiz.*, 2016, **3**, 91–112.
12 M. P. Pechini, Method for preparing lead and alkaline earth titanates and niobates and coating method using the same to form a capacitor, *US Pat.* 3330697, 1967.
13 Y. Teraoka, H. Kakebayashi, I. Moriguchi and S. Kagawa, *J. Alloys Compd.*, 1993, **193**, 70–72.
14 M. M. Natile, E. Ugel, C. Maccato and A. Glisenti, *Appl. Catal., B*, 2007, **72**, 351–362.
15 Y. Zhang-Steenwinkel, J. Beckers and A. Bliek, *Appl. Catal., A*, 2002, **235**, 79–92.
16 J. J. Kingsley and K. C. Patil, *Mater. Lett.*, 1988, **6**, 427–432.
17 A. Mali and A. Ataie, *Scr. Mater.*, 2005, **53**, 1065–1070.
18 W. Wen and J. M. Wu, *RSC Adv.*, 2014, **4**, 58090–58100.
19 B. Alkan, D. Medina, J. Landers, M. Heidelmann, U. Hagemann, S. Salamon, C. Andronescu, H. Wende, C. Schulz, W. Schuhmann and H. Wiggers, *ChemElectroChem*, 2020, **7**, 2564–2574.
20 S. Angel, J. D. Tapia, J. Gallego, U. Hagemann and H. Wiggers, *Energy Fuels*, 2021, **35**, 4367–4376.
21 G. L. Chiarello, I. Rossetti and L. Forni, *J. Catal.*, 2005, **236**, 251–261.
22 G. L. Chiarello, I. Rossetti, P. Lopinto, G. Migliavacca and L. Forni, *Catal. Today*, 2006, **117**, 549–553.
23 Y. H. Zhang, M. I. Saidaminov, I. Dursun, H. Z. Yang, B. Murali, E. Alarousu, E. Yengel, B. A. Alshankiti, O. M. Bakr and O. F. Mohammed, *J. Phys. Chem. Lett.*, 2017, **8**, 961–965.
24 W. Zheng, R. J. Sun, Y. Q. Liu, X. J. Wang, N. Q. Liu, Y. C. Ji, L. L. Wang, H. Liu and Y. H. Zhang, *ACS Appl. Mater. Interfaces*, 2021, **13**, 6404–6410.
25 B. Cai, K. Akkiraju, W. P. Mounfield, Z. S. Wang, X. Li, B. T. Huang, S. Yuan, D. Su, Y. Roman-Leshkov and Y. Shao-Horn, *Chem. Mater.*, 2019, **31**, 9422–9429.
26 F. Gonell, C. M. Sanchez-Sanchez, V. Vivier, C. Methivier, C. Laberty-Robert and D. Portehault, *Chem. Mater.*, 2020, **32**, 4241–4247.
27 Y. Q. Guo, F. C. Lei, J. D. Qi, S. S. Cao, Z. M. Wei, S. S. Lou, P. Hao, J. F. Xie and B. Tang, *ACS Sustainable Chem. Eng.*, 2020, **8**, 16711–16719.
28 A. K. Sharma, W. S. Huang, S. Pandey and H. F. Wu, *ACS Sustainable Chem. Eng.*, 2021, **9**, 7678–7686.
29 H. Ogihara, S. Masahiro, Y. Nodasaka and W. Ueda, *J. Solid State Chem.*, 2009, **182**, 1587–1592.
30 H. Ogihara, M. Sadakane, Y. Nodasaka and W. Ueda, *Chem. Mater.*, 2006, **18**, 4981–4983.
31 H. Ogihara, M. Sadakane, Y. Nodasaka and W. Ueda, *Chem. Lett.*, 2007, **36**, 258–259.
32 H. Ogihara, M. Sadakane, Q. Wu, Y. Nodasaka and W. Ueda, *Chem. Commun.*, 2007, 4047–4049, DOI: 10.1039/b708038g.
33 H. Ogihara, N. Usui, M. Yoshida-Hirahara and H. Kurokawa, *Langmuir*, 2020, **36**, 2829–2836.
34 H. Ogihara, A. Sakamaki, M. Yoshida-Hirahara and H. Kurokawa, *RSC Adv.*, 2021, **11**, 20313–20321.